processes

MDPI

Article

Numerical Simulation Study on the Thermal Efficiency of Hot Blast Stoves

Qiuchen Zhang *, Yu Tang and Lupeng Wang

School of Mechanical Engineering and Automation, Liaoning University of Technology, Jinzhou 121001, China
* Correspondence: lnzqc@163.com

Abstract: Thermal efficiency is one of the important indices used to evaluate the operational energy efficiency of hot blast stoves. In this study, a method for calculating the thermal efficiency of hot blast stoves was developed based on simulation results. The working process of top combustion hot blast stoves was numerically simulated through the established 3D fluid flow heat transfer model. The system thermal efficiency of hot blast stoves was calculated according to the simulation data, referring to the Chinese national standard, "measurement and calculation method of the heat balance of blast furnace hot blast stove" (GB/T 32287-2015). In particular, a "segmented calculation and accumulate by time" method was proposed based on the air supply curve to more precisely calculate the heat carried away by the hot blast. The results indicate that when the burning air supply cycles increased from 120 to 240 min, the thermal efficiency showed a trend of first decreasing and then increasing, with the value ranging between 70.39% and 72.48%. The reason for the decrease in thermal efficiency at a burning cycle of 150 min is explained based on heat transfer theory combined with the structural characteristics of hot blast stoves. This study provides a convenient and effective method for calculating the thermal efficiency of hot blast stoves, which helps us to evaluate and improve the operating process of hot blast stoves.

Keywords: top combustion hot blast stove; thermal efficiency; numerical simulation; combustion; air supply; heat transfer

check for updates

Citation: Zhang, Q.; Tang, Y.; Wang, L. Numerical Simulation Study on the Thermal Efficiency of Hot Blast Stoves. *Processes* **2024**, *12*, 559. https://doi.org/10.3390/pr12030559

Academic Editor: Kian Jon Chua

Received: 5 February 2024
Revised: 3 March 2024
Accepted: 8 March 2024
Published: 13 March 2024

Copyright: © 2024 by the authors. Licensee MDPI, Basel, Switzerland. This article is an open access article distributed under the terms and conditions of the Creative Commons Attribution (CC BY) license (https://creativecommons.org/licenses/by/4.0/).

1. Introduction

Hot blast stoves are critical assistive facilities for continuously providing high-temperature air (over 1200 °C) to blast furnaces in the ironmaking process. This hot air can promote pulverized coal combustion, reduce the coke ratio in ironmaking, and improve the production efficiency of blast furnaces [1–3]. At the same time, hot blast stoves are high-energy-consumption facilities, second only to blast furnaces. The amount of gas required by hot blast stoves accounts for approximately 40% of the blast furnace gas output, and their energy consumption can reach 25% of the total energy consumption [4]. Therefore, improving the hot air temperature and reducing the energy consumption of hot blast stoves are of great significance for blast furnace ironmaking. Research has shown [5] that for every 100 °C increase in the outlet air temperature, the coke ratio of the blast furnace can be reduced by 4–7%, the output can be increased by 3–5%, and the coal injection can be increased by about 40 kg per ton of iron. In recent years, many research works have been conducted to improve the hot air temperature of hot blast stoves. Zhang et al. [6] used a CFD model that was developed to simulate the combustion and heat transfer processes of top combustion hot blast stoves, creating a new record for the monthly average hot air temperature of a large blast furnace. The furnace reached 1300 °C by combining this with the multiple hot blast stove operation technologies that have been developed. Zetterholm et al. [7] studied the influence of a new OxyFuel technique on the performance of hot blast stoves based on a dynamic model of the hot blast stove system and proposed that the blast temperature could be improved by increasing the cycle time of the hot blast

stove system. Şahin and Morari [8] studied how to minimize the fuel usage of a hot blast stove system in staggered parallel operation based on a model predictive control scheme they designed. Zhong et al. [9] studied the heat transfer process of the regenerator of a self-preheating system hot blast stove using simulation methods and analyzed the heat exchange characteristics between the checker bricks and flue gas. They proposed to preheat the combustion air through the self-preheating system, which can store more heat in the regenerator and increase the air supply temperature. The research of Wei et al. [10] proved that the dual goals of high air-temperature output and low NOx emissions from hot blast stoves can be achieved by properly configuring the burner and regenerator grid bricks and adopting technologies such as optimizing the flue gas flow field.

The hot-air temperature of hot blast stoves is closely related to the thermal efficiency. Under the same burning conditions, the higher the hot-air temperature, the more effective the heat output per unit time; and the higher the thermal efficiency. Therefore, thermal efficiency is an important index for evaluating the operational energy efficiency of hot blast stoves [11,12]. The thermal efficiency of hot blast stoves is affected by many factors, including their structure, the gas type and composition, the inlet parameters of gas and combustion-supporting air, and the performance of thermal insulation and heat storage materials. In particular, the combustion state, flow field, and temperature field distribution characteristics related to the structure directly affect the heat exchange efficiency between the flue gas and the lattice bricks. In practical engineering, the thermal efficiency of hot blast stoves is usually calculated according to the Chinese national standard "measurement and calculation method of the heat balance of blast furnace hot blast stove" (GB/T 32287-2015) [13]. The thermal balance is measured through a large amount of data collected on site, and then the thermal efficiency is calculated according to the method specified by the above standard. Undoubtedly, this is an accurate and reliable calculation method. However, when using this method, manual measurement requires a large workload and a long time and cannot be applied to the adjustment of the hot blast stove process during operation. In addition, for hot blast stoves in the design stage, the data from on-site testing are unavailable due to the lack of a physical hot air stove; so thermal efficiency indicators cannot be used to evaluate the various design schemes of hot air stoves. The aim of the present work is to explore a method to calculate the thermal efficiency of hot blast stoves through simulation results without relying on on-site test data, making it possible to evaluate the energy efficiency of the hot blast stove in operation and design.

In recent years, numerical studies have been widely used to simulate the performance of specific components of hot blast stoves, such as burners and combustion chambers [14–17], regenerators [18–20], and even entire hot blast stoves [21–27]. These studies have mainly focused on the influence of the structure of hot blast stoves on the combustion, heat transfer, and turbulent processes. However, research on the thermal efficiency of hot blast stoves using numerical simulation has not been reported. Therefore, based on the top combustion hot air stoves commonly used in the ironmaking industry, in this study, a 3D fluid flow heat transfer model was established to simulate the working process of hot blast stoves. According to the obtained simulation data and referring to the Chinese national standard "measurement and calculation method of the heat balance of blast furnace hot blast stove" (GB/T 32287-2015) [13], the system thermal efficiency of hot blast stoves was calculated. The influence of the burning-air supply cycles on the thermal efficiency was analyzed.

2. Materials and Method

2.1. 3D Computational Model

Figure 1 shows the 3D calculation model of a top combustion hot blast stove equipped with a 2350 m^3 blast furnace in a steel plant. As indicated in Figure 1a, the physical model, which was drawn using Solidworks 2023 software was constructed with four sections, including the precombustion chamber, combustion chamber, regenerator, and furnace grill. The main parameters of the model were as follows: the height of the stove was 46.9 m, and

the bottom diameter of the combustion chamber was 8.8 m. The diameter and height of the regenerator were 8.3 and 26 m, respectively [23].

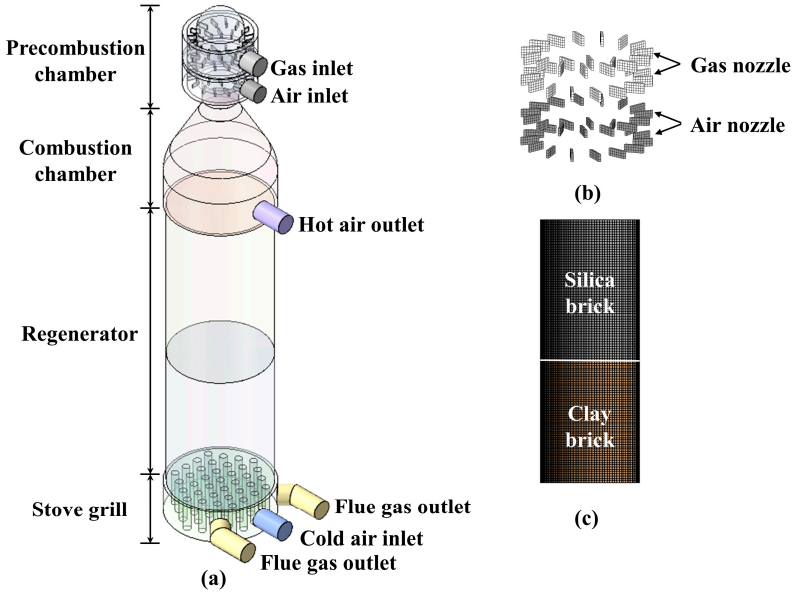

Figure 1. The 3D computational model of the top combustion hot blast stove: (**a**) physical model of hot stove; (**b**) grid of nozzles; (**c**) grid of regenerator.

The grid model of the hot blast stove was completed using Ansys Workbench 19.2 software. Given the different media presented in the hot blast stove, the computational domains were divided into the fluid domain (precombustion chamber, combustion chamber, and furnace grill) and porous medium domain (regenerator), respectively. The fluid domains were divided by a tetrahedral grid, and the regenerator was divided by a hexahedral grid. The total number of grid cells was 1,320,464, and the number of nodes was 459,278.

2.2. Mathematical Model and Computational Method

2.2.1. Mathematical Model of Numerical Simulation

The numerical model was established based on the commercial CFD package Ansys Fluent, and the corresponding mathematical models were selected for different computational domains of the hot blast stove.

- Turbulence Model

The realizable $k-\varepsilon$ two-equation model was employed to simulate the turbulent flow in the hot blast stove. The calculation equations are as follows [28,29]:

$$\frac{\partial(\rho k)}{\partial t}+\nabla\cdot\left(\rho k\vec{v}_i\right)=\nabla\cdot\left[\left(\mu+\frac{\mu_t}{\sigma_k}\right)\nabla k\right]+G_k-\rho\varepsilon, \quad (1)$$

and

$$\frac{\partial(\rho\varepsilon)}{\partial t}+\nabla\cdot\left(\rho\varepsilon\vec{v}_i\right)=\nabla\cdot\left[\left(\mu+\frac{\mu_t}{\sigma_\varepsilon}\right)\nabla\varepsilon\right]+C_{1\varepsilon}\frac{\varepsilon}{k}G_k-C_{2\varepsilon}\rho\frac{\varepsilon^2}{k}, \quad (2)$$

where ρ, $\vec{v}$ and μ represent the density, velocity vector, and dynamic viscosity of the fluid, respectively. k and ε represent the turbulence kinetic energy and dissipation rate, respectively. t represents time, G_k represents the turbulence kinetic energy. σ_k and σ_ε represent the Prandtl numbers for k and ε, respectively. In the present study, the values of the $k-\varepsilon$ mole parameters were used: $C_{1\varepsilon}=1.44$, $C_{2\varepsilon}=1.9$, $\sigma_k=1.0$ and $\sigma_\varepsilon=1.2$.

- Combustion Model

The eddy dissipation model was used to handle the combustion process of the fluid. The model assumes that the rates of chemical reaction are relatively fast compared to the turbulent mixing rate, that is, the speed control step of the combustion reaction is turbulent mixing. Therefore, the final reaction rate can be determined by the mass fraction of reactants and products. Net rate $R_{i,r}$ of component i produced by reaction r depends on the smaller one in the following two expressions:

$$R_{i,r} = \vartheta'_{i,r} M_{w,i} A \rho \frac{\varepsilon}{k} \min_R \left(\frac{Y_R}{\vartheta'_{R,r} M_{w,R}} \right), \tag{3}$$

and

$$R_{i,r} = \vartheta'_{i,r} M_{w,i} A B \rho \frac{\varepsilon}{k} \frac{\sum\limits_p Y_p}{\sum\limits_j^N \vartheta''_{j,r} M_{w,j}}, \tag{4}$$

where $\vartheta'_{i,r}$ and $\vartheta''_{i,r}$ represent the stoichiometric coefficients of the reactant and product, respectively, in chemical reaction r for component i. $M_{w,i}$ the molecular weight, ρ the mixture density, N the number of species in the system. Y_R and Y_p represent the mass fractions of the reactant R and the product P, respectively. Empirical constants $A = 4.0$ and $B = 5.0$.

- Radiation Model

In this study, the discrete ordinates (*DO*) model was selected to model the radiative heat transfer inside the hot blast stove. The *DO* model is used for complex geometries because it adopts discrete coordinates to track the radiation rays in the entire calculation domain. The radiative transfer equation can be written as [30,31]

$$\nabla \cdot (I(\vec{r}, \vec{s})\vec{s}) + (\alpha + \sigma_S) I(\vec{r}, \vec{s}) = an^2 \frac{\sigma T^4}{\pi} + \frac{\sigma_S}{4\pi} \int_0^{4\pi} I\left(\vec{r}, \vec{s}'\right) \Phi\left(\vec{s}, \vec{s}'\right) d\Omega', \tag{5}$$

where $\vec{r}$, $\vec{s}$ and $\vec{s}\prime$ represent the position, direction and scattering direction vectors, respectively. α, σ_S and n represent the spectral absorption, scattering, and refractive coefficients, respectively. I represents the radiation intensity, T represents the local temperature, Φ represents the phase function, Ω' represents the solid angle, and σ represents the Stefan-Boltzmann constant.

- Porous Media Model

The porous media model was adopted to study the heat exchange process between the checker bricks in the regenerator and high temperature flue gas and air. For a single phase flowing through porous media, the momentum and energy conservation equations can be shown as

$$\frac{\partial}{\partial t}(\gamma \rho \vec{v}) + \nabla \cdot (\gamma \rho \vec{v} \vec{v}) + \gamma \nabla p - \nabla \cdot \left[\gamma \mu \left(\nabla \vec{v} + \nabla \vec{v}^T \right) \frac{2}{3} \gamma \nabla \cdot \vec{v} \right] - \left(\frac{\mu}{\beta} + \frac{C_2 \rho}{2} |\vec{v}| \vec{v} \right) = 0, \tag{6}$$

and

$$\frac{\partial}{\partial t}\left(\gamma \rho_f E_f + (1-\gamma)\rho_S E_S\right) + \nabla \cdot \left[\vec{v}\left(\rho_f E_f + P\right)\right] = \nabla \cdot \left(k_{eff} \nabla T - \sum_i h_i \vec{J}_i \right), \tag{7}$$

where γ represents the porosity, β and C_2 represent the viscous and inertia resistance coefficients, respectively; E_f and E_S represent the total fluid and solid medium energy, respectively; ρ_f and ρ_S represent the densities of the fluid and solid, respectively; k_{eff} represents the effective conductivity [32].

2.2.2. Calculation Method of the Thermal Efficiency

The thermal efficiency of hot blast stoves refers to the percentage of their output heat and the input heat of fuel combustion, which can be divided into system thermal efficiency and body thermal efficiency. The former represents the ratio of the effective heat output of hot blast stoves to the input heat, while the latter represents the ratio of the total heat output of hot blast stoves to the input heat. Because the total heat output includes the heat loss of hot air pipes, the heat dissipation of the furnace body, and the heat removed by the cooling water, the system thermal efficiency truly reflects the utilization rate of the effective heat of hot air stoves. While the body thermal efficiency reflects the effective heat utilization rate of hot blast stoves, it also partially expresses the heat loss rate. In the present study, the focus was on the system thermal efficiency of hot blast stoves. According to the Chinese national standard "measurement and calculation method of the heat balance of blast furnace hot blast stove", the calculation formula is:

$$\eta = \frac{Q_1' - Q_4}{Q - Q_4} \times 100\%, \tag{8}$$

where Q_1' represents the heat brought out by the hot air, Q_4 represents the heat brought in by the cold air, and Q is the sum of heat received by the hot blast stove, namely

$$Q = Q_1 + Q_2 + Q_3 + Q_4, \tag{9}$$

where Q_1 represents the chemical heat generated by the gas combustion. Q_2 and Q_3 represent the physical heat brought in by the fuel and combustion supporting air, respectively. The calculation formulas for each heat are introduced below.

$$Q_1 = V_m \cdot \tau_r \cdot Q_{DW}, \tag{10}$$

where V_m represents the amount of gas used, τ_r represents the combustion period time, and Q_{DW} is the low calorific value of gas, which means the heat released by the water vapor in the combustion products cooled to 20 °C after the unit volume of gas is completely burned. For the blast furnace gas composed of various gases, the calculation formula is as follows:

$$Q_{DW} = q_{CO}\varphi_{CO} + q_{H_2}\varphi_{H_2} + \cdots, \tag{11}$$

where q_{CO}, q_{H_2} and φ_{CO}, φ_{H_2} are, respectively, the calorific value and volume fraction of each component in the gas.

$$Q_2 = V_m \cdot \tau_r \cdot (c_m \cdot t_m - c_{me} \cdot t_e), \tag{12}$$

where t_m and t_e are, respectively, the average temperatures of the fuel and the environment; c_m and c_{me} are the average specific heat capacities of the fuel at t_m and t_e, respectively.

$$Q_3 = V_m \cdot \tau_r \cdot L_n^s \cdot (c_k \cdot t_k - c_{ke} \cdot t_e), \tag{13}$$

where L_n^s represents the actual air volume required for burning 1 m^3 of gas, t_k represents the average temperature of the air; c_k and c_{ke} are the average specific heat capacities of the air at t_k and t_e, respectively.

$$Q_4 = V_f \cdot \beta \cdot (1 - L_f) \cdot \tau_f \cdot (c_f \cdot t_f - c_{fe} \cdot t_e), \tag{14}$$

where V_f represents the flow rate of the cold air, τ_f represents the air supply time, β represents the comprehensive correction coefficient of air volume, t_f represents the average temperature of the cold air, L_f represents the air leakage rate of hot blast stove. c_f and c_{fe} are the average specific heat capacities of the cold air at t_f and t_e, respectively.

$$Q_1' = V_f \cdot \beta \cdot (1 - L_f) \cdot \tau_f (c_h t_h - c_{fe} \cdot t_e), \tag{15}$$

where t_h represents the average temperature of the hot air, and c_h is the average specific heat capacity of the hot air at t_h.

2.3. Boundary Condition

In the combustion period, the inlet flow rate of the blast furnace gas was 11.83 × 10^4 $Nm^3 \cdot h^{-1}$, and the temperature was set at 423 K. Its composition is presented in Table 1 [23]. The inlet flow rate of combustion-supporting air was 7.74 × 10^4 $Nm^3 \cdot h^{-1}$, and the temperature was set at 473 K. The two exhaust gas outlets were used as the pressure boundaries, with a static pressure of 0 Pa. In the air supply period, the cold air was supplied at a flow rate of 33.42 × 10^4 $Nm^3 \cdot h^{-1}$ at 473 K. The hot air outlet was set as a pressure boundary with a static pressure of 0 Pa, and all the surface walls were considered to be as nonslip walls. As shown in Figure 1c, the regenerator consisted of two layers of checker bricks, and the physical parameters are listed in Table 2.

Table 1. Composition of blast furnace gas.

Component	CO	CO_2	H_2O	H_2	N_2
Volume fraction φ	0.24	0.19	0.023	0.01	0.537

Table 2. Parameter of checker brick [33].

Checker Brick	Density/($kg \cdot m^{-3}$)	Thermal Conductivity/($W \cdot m^{-1} \cdot K^{-1}$)	Specific Heat/($J \cdot kg^{-1} \cdot K^{-1}$)
Silica brick	1900	0.93 + 0.0007 t	794.0 + 0.251 t
Clay brick	2070	0.84 + 0.00052 t	836.8 + 0.263 t

2.4. Grid Independence Study

The grid independence study was conducted to ensure the reliability of the computational model. Based on the model with a grid number of N = 1,320,464, two new models were obtained by increasing and decreasing the number of grid cells by 20%, which were called fine grid and coarse grid according to the size of grid density, respectively. The combustion and air supply performance of three models were compared by numerical simulations under the same calculation conditions.

Because the temperature of air supply is an important indicator for evaluating the performance of hot blast stoves, the temperature curves of the hot air outlet of three stoves (as shown in Figure 2) were chosen as the object of grid independence study. The simulation results of six points in Figure 2 with an air supply temperature above 1000 °C are listed in Table 3, where "Relative error" refers to the relative error compared to the benchmark model. From Table 3, it can be seen that the change in grid number has little effect on the simulation results (with a maximum relative error of 2.23%), indicating that the used calculation model is independent of the grid.

Table 3. The results of grid independence study.

Grid Type	Parameter	Point 1	Point 2	Point 3	Point 4	Point 5	Point 6
Benchmark grid	T (°C)	1304	1294	1283	1248	1198	1110
Coarse grid	T (°C)	1296	1287	1268	1243	1177	1097
	Relative error (%)	0.62	0.58	1.16	0.39	1.75	1.11
Fine grid	T (°C)	1320	1311	1296	1275	1211	1130
	Relative error (%)	1.29	1.38	1.04	2.23	1.16	1.92

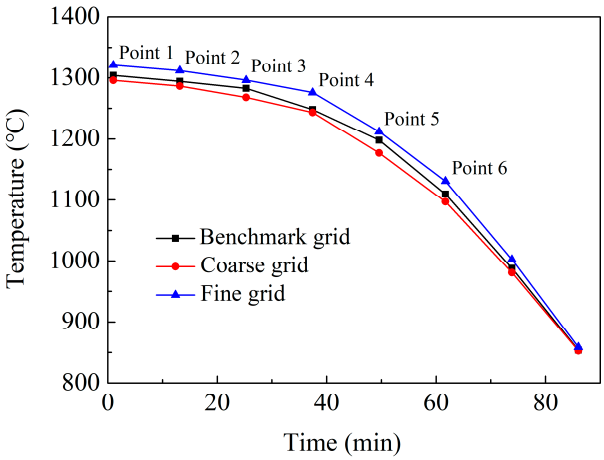

Figure 2. Temperature curves of the hot air outlet of the stoves with different grid numbers.

3. Results and Discussion

3.1. Simulation Results of the Combustion and Air Supply Periods

To systematically study the influence of different operating conditions on the thermal efficiency of hot blast stoves, simulations were conducted with burning-air supply cycles of 120, 150, 180, and 240 min, and the temperature distribution under different conditions was obtained during the combustion and air supply periods.

3.1.1. Temperature Distribution in the Combustion Period

Figure 3 shows the temperature distribution of the vertical sections of the hot blast stove at the end of different burning-air supply cycles. As shown, the temperature of the precombustion chamber was lower. This is because the gas and air nozzles were layered up and down, respectively, and the two gases did not start to mix and burn until they reached the lower part of the precombustion chamber. After the fuel gas entered the neck, the temperature constantly increased as the combustion continued. However, complete combustion only occurred in the combustion chamber, resulting in the maximum temperature of 1642 K near the dome. In the regenerator region, the layered structure of the temperature was mainly due to the upper part of the regenerator being close to the heat source, generating a higher temperature region; in the middle and lower parts, the temperature decreased gradually with the distance from the heat source and the thermal barrier effect of the upper layer. As the furnace burning time increased, the high-temperature zone of the regenerator gradually expanded, indicating that the thermal energy stored inside also increased. This temperature distribution pattern directly affected the air supply temperature and duration.

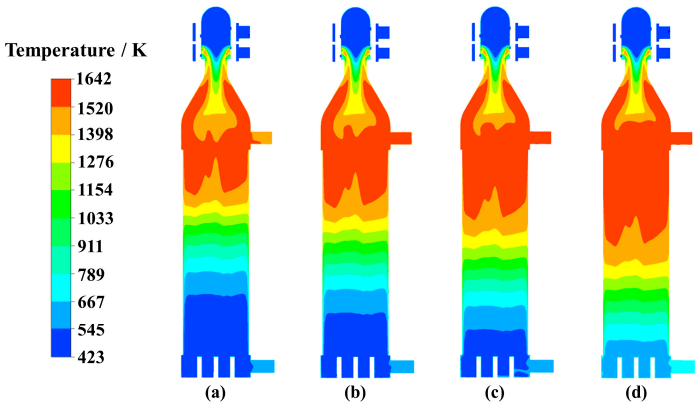

Figure 3. Temperature distribution of the stove on vertical section with different burning-air supply cycles: (**a**–**d**) 120, 150, 180, 240 min, respectively.

3.1.2. Temperature Distribution in the Air Supply Period

The air supply period of the hot air stove began after the combustion period ended, and the regenerator had stored enough heat energy. At this time, cold air entered the regenerator from the bottom of the hot blast stove, absorbed heat through heat exchange with the checker bricks, and became high-temperature hot air, which was transported to the blast furnace for ironmaking. In engineering, the effective air supply time [22] and the temperature distribution during this period are usually important indices used to evaluate the performance of hot blast stoves.

Figure 4 shows the temperature curve of the hot air outlet over time for different burning-air supply cycles. The four curves had a similar variation rule; that is, the temperature descended in a parabolic pattern. When the air temperature dropped to the lower limit of the temperature required in the project, the air supply period ended. As shown in Figure 4, the longer the furnace burning time, the higher the initial temperature of the air supply, and the longer the effective air supply time. This result corresponded to the temperature distribution in the combustion period.

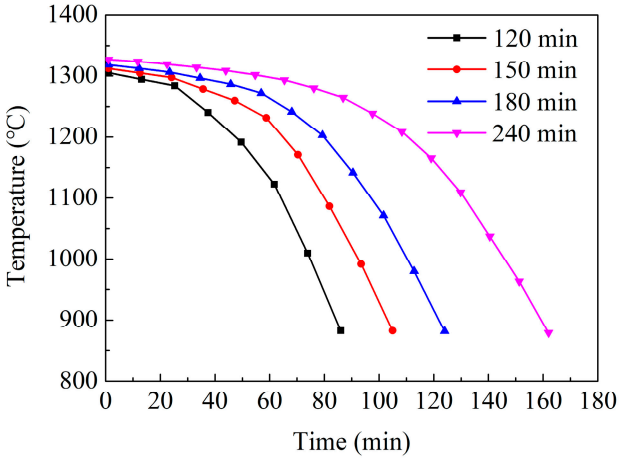

Figure 4. Temperature curves of hot air outlet with different burning-air supply cycles.

However, it is not enough to evaluate the performance of hot blast stoves solely based on the effective air supply time and the air supply temperature distribution, as they do not fully reflect the energy efficiency indicators of hot blast stoves. Only by simultaneously considering the thermal efficiency of the hot blast stove, namely, the heat transfer effect and the energy utilization efficiency, can the performance of hot blast stoves be comprehensively evaluated. Therefore, it is helpful to improve the evaluation system of hot blast stoves through calculating their thermal efficiency through numerical simulation methods.

3.2. Simulation Calculation of the Thermal Efficiency

Equations (8) and (9) calculate the thermal efficiency of hot blast stoves; the heats Q_1, Q_2, Q_3, and Q_4 are easily calculated by substituting the input and output heat of hot blast stoves obtained from the numerical simulation, as well as the relevant parameters, into the corresponding formulas. However, the calculation of heat Q_1', carried away by the hot air, is the key to the simulation methods. According to the Chinese national standard, "measurement and calculation method of the heat balance of blast furnace hot blast stove" (GB/T 32287-2015) [13], Q_1' is obtained by manually measuring the temperature, flow rate, and other parameters at the hot air outlet and then using Equation (15). The temperature t_h used in the calculation is the average temperature in the air supply period. As mentioned earlier, the temperature decrease in the air supply process is not a linear change, and in addition, the specific heat capacity of air is also a function of the temperature. If the nonlinear factors are ignored in the calculation of Q_1', and the average temperature and average specific heat capacity are used for calculation, this inevitably results in calculation

errors. Therefore, in this study, a method of calculating Q_1' was developed based on the temperature change over time curve in the air supply period.

3.2.1. The Calculation Method for Q_1'

The calculation method for Q_1' can be summarized as "segmented calculation and accumulate by time", i.e., the air supply curve was divided into several sections based on time, the heat carried by the hot air in each part was calculated separately, and then, it was summed over time. The calculation process is as follows.

In the air supply curve shown in Figure 5, the six points, a–f, are the positions of the nodes in the air supply process, where points a and f are, respectively, the starting and ending points of the effective air supply time, and $t_{h,1}$, $t_{h,2}$, …, $t_{h,5}$ represent the average temperature of each time section, respectively. In the figure, t_e is the ambient temperature. According to Figure 5, the output heat Q_{1i}' of each segmented section is calculated based on the average temperature $t_{h,i}$ of the area and the ambient temperature t_e, as well as their corresponding specific heat capacities $c_{h,i}$ and $c_{fe,i}$. By accumulating the heat output from all sections, the heat carried away by the hot air Q_1' can be calculated. According to the above scheme, the calculation Equation (15) of Q_1' is modified as

$$\begin{aligned} Q_1' &= V_f \cdot \beta \cdot (1 - L_f) \cdot \sum_{i=1}^{n} \tau_{f,i}(c_{h,i} \cdot t_{h,i} - c_{fe} \cdot t_e) \\ &= V_f \cdot \beta \cdot (1 - L_f) \cdot [\tau_{f,1}(c_{h,1} \cdot t_{h,1} - c_{fe} \cdot t_e) + \tau_{f,2}(c_{h,2} \cdot t_{h,2} - c_{fe} \cdot t_e)] \cdot \\ &+ \cdots\cdots + \tau_{f,n}(c_{h,n} \cdot t_{h,n} - c_{fe} \cdot t_e)] \end{aligned} \tag{16}$$

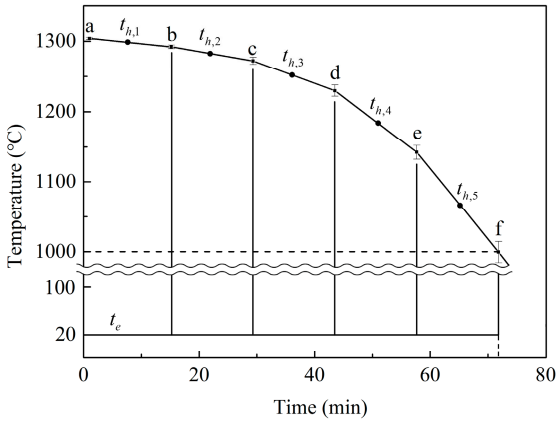

Figure 5. Schematic diagram of segmented calculation of Q_1'.

As can be seen from Equation (16), the larger the number of the nodes selected between points a and f in Figure 5, i.e., the more the sections into which the air supply curve is divided, the closer the average temperature in the interval is to the actual temperature, and the closer the calculated value of Q_1' is to the actual value. Certainly, the amount of simulation calculation is also higher. In other words, the heat Q_1' calculated by Equation (16) can more accurately reflect the thermal conditions of hot blast stoves in actual operation, and the thermal efficiency obtained from Q_1' has more practical application value.

3.2.2. Simulation Calculation Process

Considering the 120-min burning-air supply cycle as an example, the calculation process of the system thermal efficiency of hot blast stoves is introduced as follows. The mass fraction and specific heat capacity of each component of gas are summarized in Tables 4 and 5, respectively, the relevant parameters of the combustion air and cold air are shown in Table 6, and the initial conditions of the hot blast stove are shown in Table 7.

Table 4. Mass fraction of blast furnace gas.

Component	CO	CO_2	H_2O	H_2	N_2
Mass fraction ω	0.2200	0.2737	0.0136	0.0007	0.4922

Table 5. Mass specific heat capacity of gas components.

Component		CO	CO_2	H_2O	H_2	N_2
Specific heat capacity c_i/kJ·(kg·°C)$^{-1}$	t_m = 150 °C	1.044	0.888	1.884	14.387	1.042
	t_e = 20 °C	1.040	0.825	1.862	14.227	1.039

Table 6. Relevant parameters of the combustion air and cold air.

Calculation Coefficient			Inlet Temperature and Specific Heat Capacity		Ambient Temperature and Specific Heat Capacity	
L_n^s	β	L_f	$t_k\ (t_f)$ /°C	$c_k\ (c_f)$ /kJ·(m^3·°C)$^{-1}$	t_e /°C	$c_{ke}\ (c_{fe})$ /kJ·(m^3·°C)$^{-1}$
0.6549	0.98	0.03	200	1.3085	20	1.2995

Table 7. Initial conditions of hot blast stove.

Type of Gas	Flow Rate/(m^3·s^{-1})	Temperature/°C
Gas	32.8611 (V_m)	150
Cold air	92.8333 (V_f)	200

The mass fraction ω of each component in Table 4 was calculated by volume fractions φ (Table 1), and the formula is:

$$\omega_i = \varphi_i \frac{M_i}{M}, \tag{17}$$

where M_i is the molecular weight of each gas component. M is the equivalent mass of gas, which is expressed as

$$M = \sum_{i=1}^{n} M_i \varphi_i = M_{CO}\varphi_{CO} + M_{CO_2}\varphi_{CO_2} + M_{H_2O}\varphi_{H_2O} + M_{H_2}\varphi_{H_2} + M_{N_2}\varphi_{N_2}, \tag{18}$$

The mass specific heat capacity of each component in an ideal state at different temperatures was obtained from the literature. From these data, the specific heat capacity at inlet temperature t_m = 150 °C and ambient temperature t_e = 20 °C was obtained by the linear interpolation method (Table 5).

- Chemical Heat of Gas Q_1: The calorific values of CO and H_2 are 12,644 and 10,802 kJ·m^3, respectively, according to Equations (10) and (11),

$$\begin{aligned} Q_1 &= V_m \cdot \tau_r \cdot Q_{DW} = V_m \cdot \tau_r \cdot (q_{CO}\varphi_{CO} + q_{H_2}\varphi_{H_2}) \\ &= 32.8611 \times 2 \times 3600 \times (12,644 \times 24\% + 10,802 \times 1\%) = 74.3534 \times 10^7 \text{ kJ} \end{aligned}.$$

- Physical Heat of Gas Q_2: When Equation (12) is used to calculate Q_2, it is necessary to obtain the volume specific heat capacities c_m and c_{me} of the gas at the inlet and ambient temperatures t_m and t_e, respectively. The values were calculated from the mass specific heat capacity c_i in Table 5 and the density ρ_0 of the gas under the standard state.

Taking c_m of the gas at t_m = 150 °C as an example, the calculation process is:

$$\begin{aligned} M &= \sum_{i=1}^{n} M_i \varphi_i \\ &= M_{CO}\varphi_{CO} + M_{CO_2}\varphi_{CO_2} + M_{H_2O}\varphi_{H_2O} + M_{H_2}\varphi_{H_2} + M_{N_2}\varphi_{N_2} \\ &= 28 \times 24\% + 44 \times 19\% + 18 \times 2.3\% + 2 \times 1\% + 28 \times 53.7\% = 30.55 \end{aligned},$$

$$\rho_0 = \frac{M}{22.4} = \frac{30.55}{22.4} = 1.3638 \text{ kg} \cdot \text{m}^{-3},$$

and

$$\begin{aligned} c_m = \; & (c_{m,CO}\omega_{CO} + c_{m,CO_2}\omega_{CO_2} + c_{m,H_2O}\omega_{H_2O} + c_{m,H_2}\omega_{H_2} + c_{m,N_2}\omega_{N_2}) \cdot \rho_0 \\ = \; & (1.044 \times 0.2200 + 0.888 \times 0.2737 + 1.884 \times 0.0136 + 14.387 \times 0.0007 \\ & + 1.042 \times 0.4922) \times 1.3638 \\ = \; & 1.3928 \text{ kg}/(\text{m}^3 \cdot ^\circ\text{C}) \end{aligned}.$$

Similarly, the gas volume specific heat capacity $c_{me} = 1.3655$ kg/(m^3·°C) is obtained at $t_e = 20$ °C. Then, Q_2 is obtained from Equation (12):

$$\begin{aligned} Q_2 &= V_m \cdot \tau_r \cdot (c_m \cdot t_m - c_{me} \cdot t_e) \\ &= 32.8611 \times 3600 \times 2 \times (1.3928 \times 150 - 1.3655 \times 20) \\ &= 4.2968 \times 10^7 \text{ kJ} \end{aligned}.$$

- Physical Heat of Combustion Air Q_3: According to Equation (13) and the data in Table 6, the following is obtained:

$$\begin{aligned} Q_3 &= V_m \cdot \tau_r \cdot L_n^s \cdot (c_k \cdot t_k - c_{ke} \cdot t_e) \\ &= 32.8611 \times 3600 \times 2 \times 0.6549 \times (1.3085 \times 200 - 1.2995 \times 20) \\ &= 3.6523 \times 10^7 \text{ kJ} \end{aligned}.$$

- Heat Brought by Cold Air Q_4: From Equation (14) and Table 6, Q_4 is obtained:

$$\begin{aligned} Q_4 &= V_f \cdot \beta \cdot (1 - L_f) \cdot \tau_f \cdot (c_f \cdot t_f - c_{fe} \cdot t_e) \\ &= 92.8333 \times 60 \times 0.98 \times (1 - 0.03) \times 75 \times (1.3085 \times 200 - 1.2995 \times 20) \\ &= 9.3604 \times 10^7 \text{ kJ} \end{aligned}.$$

- Heat Carried by Hot Air Q_1': According to the calculation method of given above, its value is obtained by Equation (16):

$$\begin{aligned} Q_1' = \; & V_f \cdot \beta \cdot (1 - L_f) \cdot \sum_{n=1}^{n} \tau_{f,i}(c_{h,i} \cdot t_{h,i} - c_{fe} \cdot t_e) \\ = \; & V_f \cdot \beta \cdot (1 - L_f) \cdot [\tau_{f,1}(c_{h,1}t_{h,1}, -c_{fe} \cdot t_e) + \tau_{f,2}(c_{h,2} \cdot t_{h,2} - c_{fe} \cdot t_e) \\ & + \cdots + \tau_{f,n}(c_{h,n} \cdot t_{h,n} - c_{fe} \cdot t_e)] \\ = \; & 92.8333 \times 60 \times 0.98 \times (1 - 0.03) \times [1 \times (1.4447 \times 1304.9 - 1.2987 \times 20) \\ & + 26 \times (1.4435 \times 1293.45 - 1.2987 \times 20) + 30 \times (1.4351 \times 1221.5 - 1.2987 \times 20) \\ & + 3 \times (1.4275 \times 1149.5 - 1.2987 \times 20) + 15 \times (1.4262 \times 1138.0 - 1.2987 \times 20)] \\ = \; & 69.0123 \times 10^7 \text{ kJ} \end{aligned}.$$

- Total Incoming Heat Q: From Equation (9), Q is obtained:

$$\begin{aligned} Q &= Q_1 + Q_2 + Q_3 + Q_4 \\ &= (74.3534 + 4.2968 + 3.6523 + 9.3609) \times 10^7 \\ &= 91.6634 \times 10^7 \text{ kJ} \end{aligned}.$$

- System Thermal Efficiency η: For the 120-min burning-air supply cycle of the hot blast stove, the system thermal efficiency η is:

$$\eta = \frac{Q_1' - Q_4}{Q - Q_4} \times 100\% = \frac{69.0123 - 9.3604}{91.6634 - 9.3604} \times 100\% = 72.48\%.$$

3.2.3. Influence of the Burning-Air Supply Cycles on Thermal Efficiency

Using the abovementioned thermal efficiency calculation method, the input and output heat and the thermal efficiency of hot blast stoves with different burning-air supply cycles were obtained; the calculation results are listed in Table 8. Figure 6 shows the corresponding thermal efficiency curves.

Table 8. Relevant results of thermal efficiency calculation.

Time /Min	Heat Quantity $Q/10^7$ kJ					Thermal Efficiency η/%
	Q_1	Q_2	Q_3	Q_4	Q_1'	
120	74.3534	4.2968	3.6523	9.3604	69.0123	72.48
150	92.9418	5.3670	4.5613	11.4827	83.8899	70.39
180	111.5301	6.4403	5.4736	14.4158	102.5205	71.37
240	148.7068	8.5871	7.2981	19.0962	137.9696	72.22

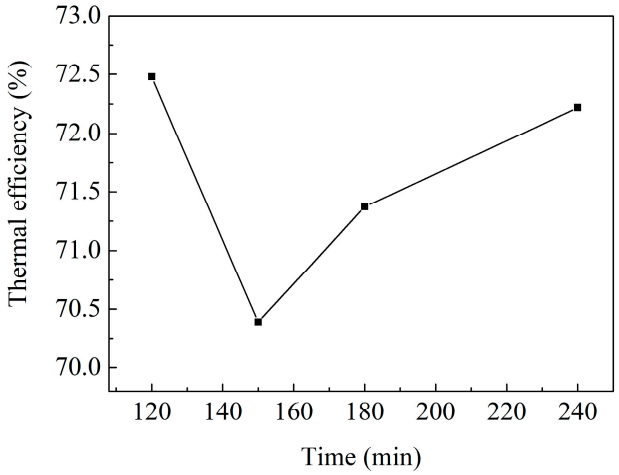

Figure 6. Thermal efficiency of different burning-air supply cycles.

In this study, the computational model used in numerical simulations has been validated by on-site testing temperature data of the hot blast stove with an average error of less than 1.5% [23]. The calculation method for thermal efficiency comes from the Chinese national standards. Therefore, the thermal efficiency calculation results obtained from simulations are credible and reliable.

As shown in Figure 6, the thermal efficiency was the highest in the 120-min burning-air supply cycle. Then, it began to decrease, reaching the lowest point at 150 min, after which it increased clearly. After 180 min, the thermal efficiency increased, but the range of change decreased. The change law of thermal efficiency can be explained as follows. In the initial stage of combustion, the unstable heat transfer process with a large temperature difference and fast heat transfer rate occurred between the upper half of the regenerator and the high-temperature flue gas from the combustion chamber. In addition to the convection heat transfer, the regenerator in this area obtained additional radiation heat transfer from the combustion chamber dome's wall surface and the combustion products in the internal space because of its proximity to the combustion chamber. This dual heat-exchange effect showed a high thermal efficiency level during the 120-min burning-air supply cycle. When the high-temperature flue gas further penetrated downward after 120-min cycles, it had to

pass through the porous channel in the upper half of the regenerator to reach the lower half. Therefore, the flow resistance was significantly increased, which affected the convection heat-exchange efficiency. In addition, due to the blocking effect of the upper heat storage body, the middle region was unable to obtain radiative heat transfer from the combustion chamber, resulting in the heat exchange in this region entering a "bottleneck period" at 150 min; so, the heat efficiency was at its lowest point. When the combustion period exceeded 150 min, the upper half of the regenerator completely entered stable heat transfer, and a large amount of high-temperature flue gas continuously penetrated downward, transferring more heat to the lower part of the middle region, gradually increasing the thermal efficiency. The air supply curves in Figure 4 show that the longer the burning-air supply cycles are, the higher the initial air supply temperature is. This is because the air supply temperature is determined by the maximum temperature, the temperature distribution and heat storage of the regenerator, and the temperature of the combustion chamber in the initial stage of the air supply. The longer the combustion time is, the higher the temperature of the combustion chamber is, the more fully the regenerator is heated by the high-temperature heat source, and the higher the initial temperature of the air supply is. However, the results in Figure 6 show that the thermal efficiency is the lowest in the 150-min burning-air supply cycle. This provides an additional reason to avoid the 150-min burning-air supply cycle when establishing a multi-stove burning-air supply operating system. In an actual project, the air supply temperature and thermal efficiency must be considered simultaneously to achieve better results.

4. Conclusions

In this study, a calculation method for the system thermal efficiency of hot blast stoves was proposed based on simulation data. The change rule of thermal efficiency in different burning-air supply cycles was analyzed. The results are summarized as follows.

(1) The system thermal efficiency of hot blast stoves was calculated based on the simulation data of combustion and air supply obtained via the ANSYS FLUENT method, referring to the Chinese national standard "Thermal Balance Measurement and Calculation Method for Blast Furnace Hot Stove". In particular, we used a "segmented calculation and accumulate by time" method based on the air supply curve to more precisely calculate the heat carried away by the hot blast. As the numerical model used in this study was validated using on-site test data, the thermal efficiency calculation method is credible and reliable.

(2) The relationship between the thermal efficiency and the burning-air supply cycles was analyzed. When the burning-air supply cycles increased from 120 to 240 min, the thermal efficiency showed a trend of first decreasing and then increasing, with values ranging between 70.39% and 72.48%. The reason for the decrease in thermal efficiency at a burning-cycle of 150 min was explained based on heat transfer theory combined with the structural characteristics of hot blast stoves.

(3) The thermal efficiency calculation method provides a convenient and effective means for evaluating the energy efficiency of hot blast stoves. It has practical significance for optimizing the design scheme and making real-time adjustments and improvements in the operating parameters of hot blast stoves.

Author Contributions: In this study, all authors were involved in the conception and design of the project. Numerical research was conducted by L.W. and Q.Z. Results analysis were completed by Y.T. The manuscript was written by Q.Z. All authors have read and agreed to the published version of the manuscript.

Funding: This study was supported by the Doctoral Starting up Foundation of Liaoning University of Technology, China (No. XB2021001).

Data Availability Statement: Data are contained within the article.

Conflicts of Interest: No conflict of interest exited in the submission of this manuscript.

Nomenclature

A, B	Empirical constant
C_2	Inertia resistance factor
$C_{1\varepsilon}$, $C_{2\varepsilon}$	Constants in the $k-\varepsilon$ two-equation
c_f, c_{fe}	Average specific heat capacities of the cold air of t_f and t_e
c_h	Average specific heat capacity of the hot air at t_h
c_k, c_{ke}	Average specific heat capacities of the air at t_k and t_e
c_m, c_{me}	Average specific heat capacities of the fuel at t_m and t_e
E_f	Total fluid energy
E_S	Total solid medium energy
G_k	Turbulence kinetic energy produced by mean velocity gradient
I	Radiation intensity
k	Turbulence kinetic energy
k_{eff}	Effective conductivity
L_f	Air leakage rate of hot blast stove
L_n^s	Actual air volume required for burning 1 m^3 of gas
M	Equivalent mass of gas
N	Number of chemical species in the system
n	Refractive coefficient
q_{CO}, q_{H_2}	Calorific values of CO and H_2 in the gas
Q	Sum of heat received by the hot blast stove
Q_1	Chemical heat generated by the gas combustion
Q_1'	Heat brought out by the hot air
Q_2	Physical heat brought in by the fuel
Q_3	Physical heat of combustion air
Q_4	Heat brought in by the cold air
Q_{DW}	Low calorific value of gas
$\vec{r}$	Position vector
$\vec{s}$	Direction vector
$\vec{s}'$	Scattering direction vectors
T	Temperature
t	Time
t_k	Average temperature of the air
t_f	Average temperature of the cold air
t_h	Average temperature of the hot air
t_m	Average temperature of the fuel
t_e	Average temperature of the environment
V_f	Flow rate of the cold air
V_m	Amount of gas
$\vec{v}$	Velocity vector
Y_P	Mass fractions of the product P
Y_R	Mass fractions of the reactant R
Greek Symbols	
α	Absorption coefficients
β	Viscous coefficients
γ	Porosity
ε	Dissipation rate
μ	Dynamic viscosity of the fluid
Ω'	Phase function
$\vartheta'_{i,r}$	Stoichiometric coefficients of reactant in chemical reaction r for component i
$\vartheta''_{i,r}$	Stoichiometric coefficients of product in chemical reaction r for component i
ρ	Density
ρ_f	Fluid density
ρ_S	Solid density

σ	Stefan-Boltzmann constant
σ_S	Scattering coefficient
σ_k, σ_ε	Prandtl numbers for k and ε
τ_f	Air supply time
τ_r	Combustion time
Φ	Phase function
φ_{CO}, φ_{H_2}	Volume fraction of CO and H_2 in the gas

References

1. Gan, Y.F.; Jang, J.Y.; Wu, T.Y. 3D dynamic thermal and thermomechanical stress analysis of a hot blast stove. *Ironmak. Steelmak.* **2020**, *47*, 959–972. [CrossRef]
2. Chen, C.; Cheng, S.; Guo, X. Hazard control of NOx in hot stove. *J. Iron Steel Res. Int.* **2014**, *21*, 306–311. [CrossRef]
3. Rieger, J.; Weiss, C.; Rummer, B. Modelling and control of pollutant formation in blast stoves. *J. Clean. Prod.* **2015**, *88*, 254–261. [CrossRef]
4. Hao, J.X.; Zhao, X.C.; Han, Y.Z.; Bai, H. Medium-term prediction model for byproduct gas consumption in hot blast stove. *China Metall.* **2018**, *28*, 17–22. (In Chinese)
5. Liu, Q. *The Operation of Blast Furnace Hot Stoves and Knowledge of Coal Gas*, 2nd ed.; Metallurgical Industry Press: Beijing, China, 2013. (In Chinese)
6. Zhang, F.; Mao, Q.; Mei, C.; Li, X.; Hu, Z. Dome combustion hot blast stove for huge blast furnace. *J. Iron Steel Res. Int.* **2012**, *19*, 1–7. [CrossRef]
7. Zetterholm, J.; Ji, X.; Sundelin, B.; Martin, P.M.; Wang, C. Dynamic modelling for the hot blast stove. *Appl. Energy* **2017**, *185*, 2142–2150. [CrossRef]
8. Şahin, A.; Morari, M. Optimizing control of hot blast stoves in staggered parallel operation. *IFAC Proc. Vol.* **2008**, *41*, 1982–1987. [CrossRef]
9. Zhong, L.; Liu, Q.; Wang, W. Computer simulation of heat transfer in regenerative chambers of self-preheating hot blast stoves. *ISIJ Int.* **2004**, *44*, 795–800. [CrossRef]
10. Wei, Q.; Ge, L.; Liu, S.; Fu, Z.; Cheng, S.; Wang, L.; Liu, L. High air temperature and low nitrogen combustion technology of top burning catenary hot blast stove. *Heibei Metall.* **2021**, *2*, 64–68. (In Chinese)
11. Cui, G.; Wei, Y. Optimization of hot blast stove combustion control based on pattern matching. *Metall. Ind. Autom.* **2015**, *39*, 69–72. (In Chinese)
12. Zhang, B.; Niu, H.; Geng, X.; Lou, Q. Design and application of thermal efficiency calculation module for hot blast stove. *Metall. Ind. Autom.* **2019**, *43*, 34–38+57. (In Chinese)
13. *GB/T 32287-2015*; Method of Determination and Calculation of Heat Balance for Hot Stove in Blast Furnace. The Technical Committee on Steel of Standardization Committee of China: Beijing, China, 2015. (In Chinese)
14. Zhao, M.; Pan, Y.; Meng, F.; Ma, P.; Jia, L. CFD numerical simulation of operation for energy saving during combustion period of Kalugin top combustion. *Trans. Indian Inst. Met.* **2023**, *76*, 1967–1976. [CrossRef]
15. Guo, H.; Yan, B.; Zhang, J.; Liu, F.; Pei, Y. Optimization of the number of burner nozzles in a hot blast stove by the way of simulation. *JOM* **2014**, *66*, 1241–1252. [CrossRef]
16. Hao, X.; Zhang, Z.; Zhang, S.; Bo, F. Research on combustion characteristics of top combustion hot blast stove by radial angle of nozzle. *Ind. Heat.* **2018**, *47*, 8–11+16. (In Chinese)
17. Chen, S.; Guo, H.; Zhang, J.; Yang, T. Combustion model of a hot blast stove based on numerical simulation. *J. Univ. Sci. Technol. Beijing* **2011**, *33*, 627–631. (In Chinese)
18. Kimura, Y.; Takatani, K.; Otsu, N. Three-dimensional mathematical modeling and designing of hot stove. *ISIJ Int.* **2010**, *50*, 1040–1047. [CrossRef]
19. Chen, C.; Cheng, S.; Guo, X. Heat transfer parameters of gas inside grid bricks of hot blast stove. *Chin. Process Eng.* **2012**, *12*, 765–769. (In Chinese)
20. Zhao, M.; Pan, Y.; Meng, F.; Ma, P. Rapid prediction of hot-air temperature of Kalugin top combustion hot blast stove by means of computational fluid dynamics numerical simulation. *Metals* **2023**, *13*, 1623. [CrossRef]
21. Qi, F.; Liu, Z.; Yao, C.; Li, B. Numerical study and structural optimization of a top combustion hot blast stove. *Adv. Mech. Eng.* **2015**, *7*, 709675. [CrossRef]
22. Zhang, Q.; Chen, L.; Ma, X.; Zhao, C. Numerical study of combustion and air supply characteristics and structural optimization of top combustion hot blast stoves. *ISIJ Int.* **2021**, *61*, 62–70. [CrossRef]
23. Zhang, Q.; Chen, L.; Zhao, C. Numerical simulation of combustion and air supply process and optimal design of traditional top combustion hot blast stoves. *Steel Res. Int.* **2021**, *92*, 2000311. [CrossRef]
24. Zhao, C.; Chen, L. numerical study on periodic work of a top combustion hot blast stove. *China Metall.* **2021**, *31*, 132–1377. (In Chinese)
25. Yan, K.; Cheng, S. Stress and deformation analysis of top combustion hot blast stove shell. In *The Minerals, Metals and Materials Series (TMS) 2017*; Springer: San Diego, CA, USA, 2017; pp. 757–765.

26. Jiang, Z.; Zhou, G.; Zhang, H.; Gui, W.; Yang, C.; Xie, Y. Temperature distribution model for combustion process of hot blast stove of dome combustion ball type. *J. Cent. South Univ.* **2018**, *49*, 2216–2224. (In Chinese)
27. Matino, I.; Dettori, S.; Colla, V.; Weber, V.; Salame, S. Two innovative modelling approaches in order to forecast consumption of blast furnace gas by hot blast stoves. *Energy Procedia* **2019**, *158*, 4043–4048. [CrossRef]
28. Launder, B.E.; Spalding, D.B. The numerical computation of turbulent flows. *Comp. Methods Appl. Mech. Eng.* **1974**, *3*, 269–289. [CrossRef]
29. Veynante, D.; Vervisch, L. Turbulent combustion modeling. *Prog. Energ. Combust.* **2002**, *28*, 193–266. [CrossRef]
30. Coelho, P.J. Numerical simulation of the interaction between turbulence and radiation in reactive flows. *Prog. Energ. Combust.* **2007**, *33*, 311–383. [CrossRef]
31. Keramida, E.P.; Liakos, H.H.; Founti, M.A.; Boudouvis, A.G.; Markatos, N.C. Radiative heat transfer in natural gas-fired furnaces. *Int. J. Heat Mass Transf.* **2000**, *43*, 1801–1809. [CrossRef]
32. Kuwahara, F.; Nakayama, A.; Koyama, H. A Numerical study of thermal dispersion in porous media. *J. Heat Transf.* **1996**, *118*, 756–761. [CrossRef]
33. Cheng, L. *Ironmaking Process and Calculation in Blast Furnace*; Metallurgical Industry Press: Beijing, China, 1991. (In Chinese)

Disclaimer/Publisher's Note: The statements, opinions and data contained in all publications are solely those of the individual author(s) and contributor(s) and not of MDPI and/or the editor(s). MDPI and/or the editor(s) disclaim responsibility for any injury to people or property resulting from any ideas, methods, instructions or products referred to in the content.